Differential absorption lidar for volcanic CO_2 sensing tested in an unstable atmosphere

Manuel Queißer,[1,*] Mike Burton,[1] and Luca Fiorani[2]

[1]*Istituto Nazionale di Geofisica e Vulcanologia (INGV), Sezione di Pisa, 56126 Pisa, Italy*
[2]*Italian National Agency for New Technologies, Energy and Sustainable Economic Development (ENEA), 00044 Frascati, Italy*
[*]*manuelqueisser@web.de*

Abstract: Motivated by the need for an extremely durable and portable instrument to quantify volcanic CO_2 we have produced a corresponding differential absorption lidar (DIAL). It was tested on a volcano (Vulcano, Italy), sensing a non-uniform volcanic CO_2 signal under turbulent atmospheric conditions. The measured CO_2 mixing ratio trend agrees qualitatively well but quantitatively poorly with a reference CO_2 measurement. The disagreement is not in line with the precision of the DIAL determined under conditions that largely exclude atmospheric effects. We show evidence that the disagreement is mainly due to atmospheric turbulence. We conclude that excluding noise associated with atmospheric turbulence, as commonly done in precision analysis of DIAL instruments, may largely underestimate the error of measured CO_2 concentrations in turbulent atmospheric conditions. Implications for volcanic CO_2 sensing with DIAL are outlined.

OCIS codes: (010.3640) Lidar; (280.1910) DIAL, differential absorption lidar.

References and links

1. T. Gerlach, "Volcanic versus anthropogenic carbon dioxide," Eos Trans. AGU **92**(24), 201–202 (2011).
2. M. R. Burton, G. M. Sawyer, and D. Granieri, "Deep carbon emissions from Volcanoes," Rev. Mineral. Geochem. **75**(1), 323–354 (2013).
3. N. Menyuk, D. K. Killinger, and W. E. Defeo, "Remote sensing of NO using a differential absorption lidar," Appl. Opt. **19**(19), 3282–3286 (1980).
4. T. Hamazaki, A. Kuze, and K. Kondo, "Sensor system for greenhouse gas observing satellite (GOSAT)," Proc. SPIE **5543**, 275–282 (2004).
5. J. Abshire, H. Riris, G. R. Allan, C. J. Weaver, J. Mao, X. Sun, W. E. Hasselbrack, S. R. Kawa, and S. Biraud, "Pulsed airborne lidar measurements of atmospheric CO_2 column absorption," Tellus **62**(5), 770–783 (2010).
6. G. D. Spiers, R. T. Menzies, J. Jacob, L. E. Christensen, M. W. Phillips, Y. Choi, and E. V. Browell, "Atmospheric CO_2 measurements with a 2 μm airborne laser absorption spectrometer employing coherent detection," Appl. Opt. **50**(14), 2098–2111 (2011).
7. J. T. Dobler, F. W. Harrison, E. V. Browell, B. Lin, D. McGregor, S. Kooi, Y. Choi, and S. Ismail, "Atmospheric CO_2 column measurements with an airborne intensity-modulated continuous wave 1.57 μm fiber laser lidar," Appl. Opt. **52**(12), 2874–2892 (2013).
8. D. Sakaizawa, C. Nagasawa, T. Nagai, M. Abo, Y. Shibata, M. Nakazato, and T. Sakai, "Development of a 1.6 μm differential absorption lidar with a quasi-phase-matching optical parametric oscillator photon-counting detector for the vertical CO_2 profile," Appl. Opt. **48**(4), 748–757 (2009).
9. W. Johnson, K. S. Repasky, and J. L. Carlsten, "Micropulse differential absorption lidar for identification of carbon sequestration site leakage," Appl. Opt. **52**(13), 2994–3003 (2013).
10. S. Kameyama, M. Imaki, Y. Hirano, S. Ueno, S. Kawakami, D. Sakaizawa, and M. Nakajima, "Development of 1.6 μm continuous-wave modulation hard-target differential absorption lidar system for CO_2 sensing," Opt. Lett. **34**(10), 1513–1515 (2009).
11. H. Liu, T. Chen, R. Shu, G. Hong, L. Zheng, Y. Ge, and Y. Hu, "Wavelength-locking-free 1.57 μm differential absorption lidar for CO_2 sensing," Opt. Express **22**(22), 27675–27680 (2014).
12. A. Amediek, A. Fix, M. Wirth, and G. Ehret, "Development of an OPO system at 1.57 μm for integrated path DIAL measurement of atmospheric carbon dioxide," Appl. Phys. B **92**(2), 295–302 (2008).
13. L. S. Rothman, I. E. Gordon, Y. Babikov, A. Barbe, D. C. Benner, P. F. Bernath, M. Birk, L. Bizzocchi, V. Boudon, L. R. Brown, A. Campargue, K. Chanc, L. Coudert, V. M. Devi, B. J. Drouin, A. Fayt, J.-M. Flaud, R. R. Gamache, J. Harrison, J.-M. Hartmann, C. Hill, J. T. Hodges, D. Jacquemart, A. Jolly, J. Lamouroux, R. L. LeRoy, G. Li, D. Long, C. J. Mackie, S. T. Massie, S. Mikhailenko, H. S. P. Müller, O. V. Naumenko, A. V.

#227072 - $15.00 USD Received 19 Nov 2014; revised 3 Jan 2015; accepted 3 Jan 2015; published 3 Mar 2015

Nikitin, J. Orphal, V. Perevalov, A. Perrin, E. R. Polovtseva, C. Richard, M. A. H. Smith, E. Starikova, K. Sung, S. Tashkun, J. Tennyson, G. C. Toon, V. G. Tyuterev, J. V. Auwera, and G. Wagner, "The HITRAN 2012 molecular spectroscopic database," J. Quant. Spectrosc. Radiat. Transf. **130**, 4–50 (2013).
14. H. Riris, M. Rodriguez, G. R. Allan, W. Hasselbrack, J. Mao, M. Stephen, and J. Abshire, "Pulsed airborne lidar measurements of atmospheric optical depth using the Oxygen A-band at 765 nm," Appl. Opt. **52**(25), 6369–6382 (2013).
15. R. M. Schottland, "Errors in the lidar measurement of atmospheric gases by differential absorption," J. Appl. Meteorol. **13**(1), 71–77 (1974).
16. L. Fiorani and E. Durieux, "Comparison among error calculations in differential absorption lidar measurements," Opt. Laser Technol. **33**(6), 371–377 (2001).
17. S. Yin and W. Wang, "Effect of atmospheric scintillation on SNR of differential absorption lidar system," J. Electr. Sci. Technol. China **2**, 21–24 (2004).
18. A. S. Gurvich and S. S. Kashkarov, "Problem of enhancement of scattering in a turbulent medium," Radiophys. Quantum Electron. **20**(5), 547–549 (1977).
19. X. Sun and J. B. Abshire, "Comparison of IPDA lidar receiver sensitivity for coherent detection and for direct detection using sine-wave and pulsed modulation," Opt. Express **20**(19), 21291–21304 (2012).
20. W. B. Grant, A. M. Brothers, and J. R. Bogan, "Differential absorption lidar signal averaging," Appl. Opt. **27**(10), 1934–1938 (1988).
21. G. P. Berman, V. N. Gorshkov, and S. V. Torous, "Scintillation reduction for laser beams propagating through turbulent atmosphere," J. Phys. At. Mol. Opt. Phys. **44**(5), 055402 (2011).
22. J. Chrzanowski, J. Kirkiewicz, and Y. A. Kravtsov, "Influence of enhanced backscattering phenomenon on laser measurements of dust and aerosols content in a turbulent atmosphere," Phys. Lett. A **300**(2-3), 298–302 (2002).
23. D. H. Tofsted, S. G. O'Brien, and G. T. Vaucher, "An atmospheric profile model for use in army wargaming applications 1," U.S. Army Research Laboratory, report ARL-TR-3748, 2006.
24. W. B. Grant, "He-Ne and cw CO_2 laser long-path systems for gas detection," Appl. Opt. **25**(5), 709–719 (1986).
25. A. Aiuppa, S. Inguaggiato, A. J. S. McGonigle, M. O'Dwyer, C. Oppenheimer, M. J. Padgett, D. Rouwet, and M. Valenza, "H_2S fluxes from Mt. Etna, Stromboli, and Vulcano (Italy) and implications for the sulfur budget at volcanoes," Geochim. Cosmochim. Acta **69**(7), 1861–1871 (2005).
26. M. R. Burton, C. Oppenheimer, L. A. Horrocks, and P. W. Francis, "Remote sensing of CO_2 and H_2O emission rates from Masaya volcano, Nicaragua," Geology **28**(10), 915–918 (2000).
27. A. Marshak, J. V. Martins, V. Zubko, and Y. J. Kaufman, "What does reflection from cloud sides tell us about vertical distribution of cloud droplet sizes?" Atmos. Chem. Phys. **6**(12), 5295–5305 (2006).
28. D. Masiyano, J. Hodgkinson, and R. P. Tatam, "Use of diffuse reflections in tunable diode laser absorption spectroscopy: implications of laser speckle for gas absorption measurements," Appl. Phys. B **90**(2), 279–288 (2008).
29. C. W. Higgins, M. Froidevaux, V. Simeonov, N. Vercauteren, C. Barry, and M. B. Parlange, "The effect of scale on the applicability of taylor's frozen turbulence hypothesis in the atmospheric boundary layer," Bound.-Layer Meteor. **143**(2), 379–391 (2012).

1. Introduction

Volcanoes are an important natural source of CO_2 in the global geochemical carbon cycle, contributing 1-5% relative to anthropogenic amounts [1,2]. To better understand the carbon cycle a direct measurement of the CO_2 flux from sub-aerial volcanoes is desirable. This is the main target of the ongoing European Research Council (ERC) project CO_2Volc. Since many volcanoes are hazardous and remote an optimal instrument should operate remotely.

Differential absorption lidar (DIAL) is a remote sensing platform, which has already been used in the 1980ies to quantify atmospheric gases [3]. Nowadays, numerous groups worldwide are working on the development of DIAL based remote sensing techniques to quantify atmospheric CO_2, mostly of the background. They are often developed for the use on airborne platforms or towards satellite missions [4–7]. Many of the approaches measure light scattered back from a hard target, such as the ground, which yields column averaged CO_2 concentrations, a technique called integrated path differential absorption (IPDA). Range resolved CO_2 concentrations have been retrieved as well with DIAL [8,9].

Measuring volcanic CO_2 has some particular characteristics, which require a fit for purpose design. An advantage is that in order to measure volcanic CO_2 the required path length would be relatively short, lowering the required average optical power. However, a smaller column length along with a rather modest volcanic CO_2 signal [2] means less molecular absorption, challenging the instrument's precision. The precision must allow to sense a volcanic CO_2 signal of around 50 parts per million (ppm) within a 200 m thick plume inside a 1000 m path with ca. 30% error. This corresponds to an error of the average CO_2 mixing ratio of a few ppm for a 1000 m path length. As many volcanoes are mountains, the

#227072 - $15.00 USD Received 19 Nov 2014; revised 3 Jan 2015; accepted 3 Jan 2015; published 3 Mar 2015

atmospheric conditions at a volcanic site are typically very complex and dynamic. For instance, depending on the wind conditions the plume direction may vary by a couple of degrees every few seconds. This requires an instrument that can be easily transported, set up in a flexible manner and is ready to measure quickly. Whilst some volcanoes allow for a ground based horizontal measurement near the crater, others may require a measurement vertically downwards through the plume from an aircraft or upwards from a moving car. All this stands in need for a very portable, rugged, lightweight yet precise instrument, dedicated as a volcanology tool, i.e. easy to use. With these constraints in mind we have designed and built a prototype of a compact DIAL based on IPDA.

Many of the works on DIAL sensing CO_2 do not include the influence of atmospheric effects in the precision analysis [5,8,9]. In some cases the precision is measured, but atmospheric effects are excluded in the test setup [10]. The precision analysis is commonly followed by verification where measured CO_2 concentrations associated with laser propagation through a column are compared to in situ reference measurements [5,9,10]. However, for a measurement path containing a non-uniform CO_2 concentration and in an unstable atmosphere this practice may lead to disagreement with the reference measurement [11].

In consonance with this we present and discuss evidence that due to turbulent atmospheric conditions CO_2 concentrations measured by the compact DIAL on a volcano (Vulcano, Italy) compare qualitatively but not quantitatively to an in situ measurement. This means that excluding atmospheric effects in precision characterization of a DIAL may largely underestimate the error of measured CO_2 concentration in turbulent atmospheric conditions. This has important implications to remote sensing of volcanic CO_2 with DIAL.

2. Basic principles

The compact DIAL operates at two wavelengths. One of the wavelengths is tuned to the maximum of an absorption line of the CO_2 molecule (hereafter referred to as ON wavelength), the other wavelength is set close to the absorption line, where there is no absorption by CO_2 (hereafter referred to as OFF wavelength). We chose 1572.992 nm (ON) and 1573.160 nm (OFF) since the corresponding water vapor absorption strengths are equal and no bias is added to the retrieved CO_2 concentration [12]. Moreover, the line strength shows very little dependence on temperature [13]. The column averaged CO_2 concentration N can be expressed as [5]

$$N = \frac{DOD}{\Delta\sigma R}, \tag{1}$$

where

$$DOD = -\frac{1}{2}\ln\left(\frac{P_{ON}P_{OFF,ref}}{P_{OFF}P_{ON,ref}}\right) \tag{2}$$

is the differential optical depth. P_{ON} and P_{OFF} are the received optical powers associated with the ON and OFF wavelengths, respectively. $P_{ON,ref}$ and $P_{OFF,ref}$ are the transmitted optical powers for the ON and OFF wavelengths, respectively, used to normalize power fluctuations of the transmitter. R is the distance between the instrument and the hard target and defines the measurement column. $\Delta\sigma$ is the differential molecular absorption cross section of CO_2. Note that in Eq. (1) we assume a constant air number density along R, which is reasonable for a horizontal path. The key measurement parameter is represented by the ratio of the normalized signals (power or voltage) in Eq. (2) and is called the grand ratio (GR).

Equation (1) assumes that P_{ON} and P_{OFF} only differ due to CO_2 absorption. However, differences in the instrument related optical depths for the ON and OFF wavelengths due to etalon fringes occurring in the optical components, e.g. the detector interface, lead to a wavelength depending signal strength. This internal etalon effect causes a slight offset (systematic error) of the GR. Moreover, the GR may vary in a non-stationary manner due to

#227072 - $15.00 USD Received 19 Nov 2014; revised 3 Jan 2015; accepted 3 Jan 2015; published 3 Mar 2015

changes in temperature, pressure, mechanical vibrations and other factors [14]. Other than systematic errors, for the compact DIAL the following statistical noise sources are relevant: laser noise, detector related noise (e.g. dark current, shot noise, trans impedance amplifier (TIA) noise), solar background noise, noise due to atmospheric turbulence and reflective speckle noise. By employing an interference filter, solar background noise is effectively reduced. Atmospheric turbulence may represent a significant source of noise for lidar and DIAL in the open atmosphere [15–17]. Also called turbulence-induced enhanced backscattering, it was first observed in 1977 [18]. Turbulent air currents randomly alter the refractive index structure of air along the beam, causing beam wandering and wave front distortion, which give rise to an unevenly distributed irradiance, termed scintillation. The speckle pattern upon hard target reflection is random, but repeatable for an immobile geometry, therefore adding a bias to the GR. Noise due to reflective speckle can be kept small provided sufficient spatial or temporal averaging of speckles [19]. Under turbulent conditions reflective speckle and atmospheric influences, although uncorrelated [17], generally have a combined effect [20]. This is easily understood, since the rough target is illuminated in a geometrically random fashion. Moreover, as the DIAL beam propagates back to the receiver the speckle pattern is randomly altered, since the turbulent atmosphere can be modeled as a series of random phase screens [21]. A treatment of the latter kind is necessary to account for that combined effect, but out of the scope of this work. Therefore, in the following speckle noise estimations assume a calm atmosphere with zero turbulence. Vice versa, purely turbulence related noise is assessed by neglecting speckle.

3. Instrument realization and characterization

Figure 1(a) shows a block diagram of the compact DIAL prototype. The laser system comprises of two continuous wave (cw) distributed feedback (DFB) fiber seed lasers and an Erbium doped fiber amplifier (EDFA) from NKT photonics. The cw approach implies that the instrument measures column averaged CO_2 concentrations. This suffices as the background CO_2 concentration is obtained implicitly since for a flux measurement a scan across the volcanic plume has to be made, which includes the atmosphere outside the plume. The fiber lasers have low weight and small dimensions. The complete prototype weighs ca. 20 kg. If necessary it can be transported in two backpacks through rough terrain. Another benefit in terms of producing a field portable instrument is the lower level of maintenance required compared with instruments using pulsed lasers.

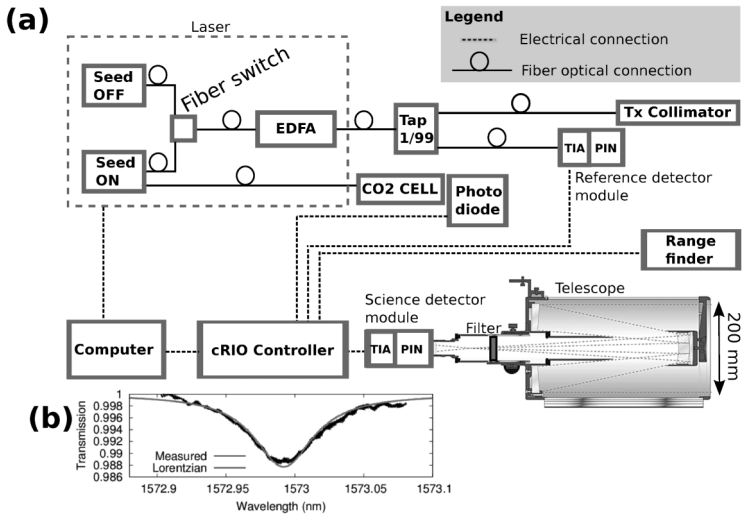

Fig. 1. (a) System configuration of the compact DIAL. (b) Absorption spectrum from the reference CO_2 cell made with the ON seed laser. The grey curve depicts the transmission computed assuming a Lorentzian absorption line shape.

#227072 - $15.00 USD Received 19 Nov 2014; revised 3 Jan 2015; accepted 3 Jan 2015; published 3 Mar 2015

The EDFA possesses good heat dissipation and has low electrical power consumption. The instrument is powered by a lithium polymer battery and uses ~20 W in idle mode (amplifier off) and ~70 W when the amplifier is working at its full optical power of 1.5 W. The intensity noise of the laser is low compared with the detector noise and can be neglected. Thanks to the narrow line width of the seed laser wavelengths (< 1 ppm of CO_2 absorption line width) there is practically no associated error in CO_2 concentration. For each seed laser, software controlled thermal expansion or contraction of the fiber allows to fix the wavelength at a set point and permits tuning by ca. +/– 300 pm around the absorption line center, allowing to scan the CO_2 absorption line. This is used to calibrate the seed laser wavelengths. For the ON wavelength, a fraction of the seed laser light is tapped and passes a 100 mm long reference absorption cell containing pure CO_2 at a pressure of 1 atm [Fig. 1(b)].

The manufacturer specifies the wavelength stability to be below 0.04 pm/hour by measuring the beat frequency of the wavelength of two identical seed laser modules. We find that by repeatedly measuring absorption spectra using an absorption cell the wavelength is within a root mean square (RMS) of 0.6 pm, which corresponds to ca. 1% of the absorption line width, for at least 30 min. This method is less precise than the beat frequency method. Thus, 0.6 pm can be seen as an upper stability limit. For most volcanic plume diameters (20 - 200 m) and volcanic CO_2 concentrations (> 20 ppm) this wavelength stability would lead to an error of the volcanic CO_2 concentration of less than 1%.

To measure the hard target distance R we use a military range finder lidar with 50 cm accuracy. The wavelength is 1550 nm and hence close to the ON and OFF wavelengths, which means the propagation effects are similar.

A fiber switch with less than 300 ns rise time ensures that only photons of either ON or OFF wavelength at a time pass the EDFA. The switch operates at a maximum switching rate of 2 kHz, limited by the band pass filter of the detector module. After the fiber amplifier 1% of the light power is tapped and measured by a reference InGaAs PIN detector module. The reference signal is used to normalize the science signal to correct for fluctuations of the laser power. In order to minimize normalization residuals, the reference detector module is the same model as the science detector module (Femto OS-200-IN2). 99% of the light is passed to the collimator that has a maximized divergence of 1.7 mrad to effectively average speckles.

To avoid errors due to polarization dependent transmission and target reflectivity, all fibers in the transmitter unit, including the lasers, are of the polarization maintaining type.

The transmitter/telescope arrangement is biaxial, which helps to reduce noise due to turbulence-enhanced backscattering [22]. For practical reasons the light from the telescope passes the filter slightly off-normally, under ca. 3 degrees, leading to a decrease in central wavelength by less than 0.8 nm. The science PIN detector module is directly mounted behind the telescope to minimize transmission losses. Good thermal coupling of the detectors, fiber sleeves etc. with a common aluminum instrument frame helps reducing thermal gradients and thus drift of the GR. To further minimize interference related noise we use anti-reflection coated optics and angled fiber connectors wherever feasible.

The voltages provided by the TIAs of the science and reference detector modules are simultaneously sampled by a 24-bit analog to digital converter (ADC) at a rate of 50 kSamples/s. A Compact Rio (cRIO) controller from National Instruments manages the acquired data, including the range finder data, and streams them to the host computer for processing via first in, first out (FIFO). At 2 kHz wavelength switching rate 25 samples per ON and 25 samples per OFF state are being acquired, hence 50 samples per science and 50 samples per reference ON/OFF pair. This corresponds to a total integration time of 1 ms.

In a fiber-closed loop setup, if both seed lasers are emitting at the same wavelength, the low digitization noise of the 24-bit ADC allows detector noise limited acquisition with a signal to noise ratio (SNR) of the order of 10^5. Once the wavelengths are set to their default values the SNR is limited by drift of the GR related to the internal etalon effect. However, after the system has warmed up the bias variation is similar for the science and reference signals, resulting in a stable GR. For a 22 m path in the closed laboratory, using a wall as a target, the measured GR precision (standard deviation, STD) is 0.00176 (0.015 dB), for at

#227072 - $15.00 USD Received 19 Nov 2014; revised 3 Jan 2015; accepted 3 Jan 2015; published 3 Mar 2015

least 15 min (Fig. 2). This is long enough for the envisaged acquisition in the field since each measurement is preceded by a calibration test.

Since we are interested in the relative change due to volcanic CO_2, provided it does not drift significantly a GR offset as in Fig. 2 does not pose a problem. If the offset is desired, a technique we propose is to place a high surface quality retro-reflector close enough to the telescope to minimize atmospheric effects, but far enough for a sufficiently large beam diameter in order to minimize bias due to speckle noise. A feasible distance for the parameters of the compact DIAL is ca. 40 m. Then the GR and its offset can be measured, while one has to correct for the CO_2 absorption within the 40 m path. Since the path length is small the latter can be measured in situ.

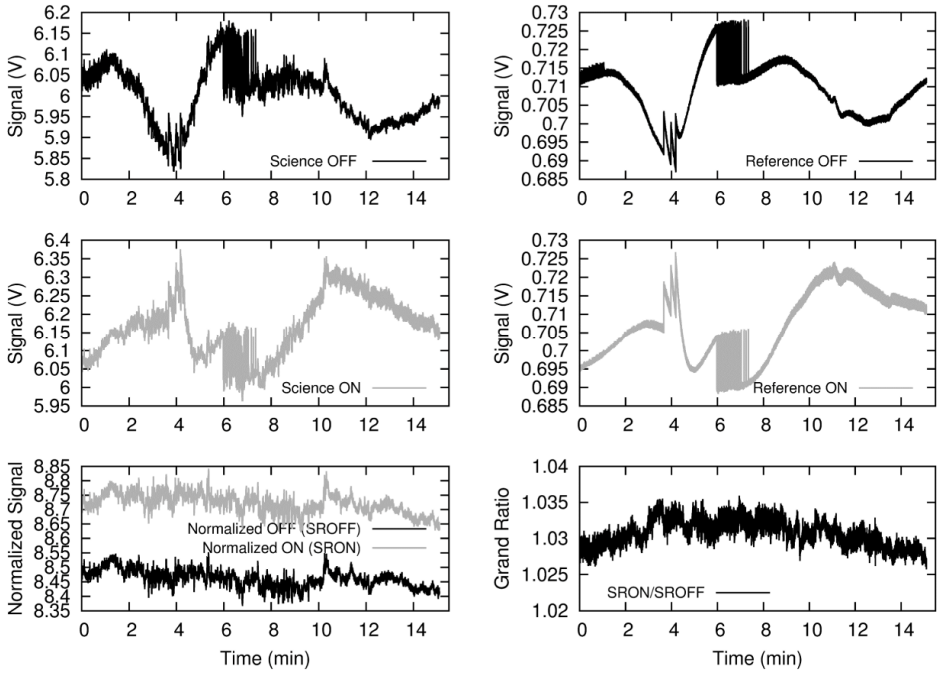

Fig. 2. Laboratory calibration test at 22 m target distance with a wavelength switching rate of 2 kHz. SRON and SROFF depict the normalized ON and OFF science signal, respectively. The standard deviation of the GR is 0.00176 or 0.015 dB. The offset of the GR is 0.03.

To verify the sensitivity of the instrument to CO_2 we introduced a known amount of CO_2 along the beam path inside the laboratory. To confine the CO_2, a box covering the beam was installed at the hard target (wall) at 22 m distance. Only the beam entrance side was open, while the exit side was closed by the hard target. The box had a length of 50 cm and a volume of 90 metric liters (l). A moderate flush of CO_2 introduced ~2 l of pure CO_2 from the top of the box. Assuming that the CO_2 well mixed with the air inside the box this would correspond to an absorption of ca. 1%, or a change in GR by ca. 0.01, as shown in Fig. 3(a).

#227072 - $15.00 USD Received 19 Nov 2014; revised 3 Jan 2015; accepted 3 Jan 2015; published 3 Mar 2015

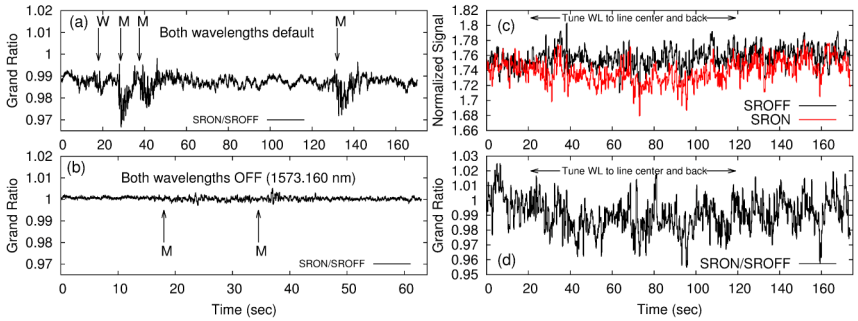

Fig. 3. (a) Indoor sensitivity test. The wavelength switching rate was 1 kHz. W depicts weak flush (CO_2 volume ~2/3 l), M depicts moderate flush (CO_2 volume ~2 l). The arrows mark the start of the flushes. Each flush took ca. 2 seconds. Wavelengths at default. (b) Repeated test with both wavelengths set to OFF. (c) Normalized science signals during an outdoor sensitivity test. The wavelength switching rate was 500 Hz. (d) GR (Ratio between SRON and SROFF in Fig. 3(c)).

A weak flush introduced ~2/3 l, which gives rise to an expected GR change by ca. 0.004. To further substantiate the result, both seed laser wavelengths were tuned to the OFF wavelength so that the expected as well as the observed CO_2 absorption was zero [Fig. 3(b)]. Figure 3(b) also shows how the GR offset vanishes once both seed laser wavelengths are equal. Moreover, the signal exhibits less noise than in Fig. 3(a), since interferometric effects are removed and the associated residuals in the normalized science signals (SRON, SROFF) are reduced. Figures 3(c) and 3(d) show the normalized science signals and the GR, respectively, of an outdoor sensitivity test using the natural background CO_2. The hard target was a concrete wall at 100 m distance. Assuming a background CO_2 concentration of 390 ppm the expected CO_2 absorbance is 1%, corresponding to a change in GR by ca. 0.01. Until 21 s both seed lasers emitted at the OFF wavelength. After that one of them was tuned to the ON wavelength and at 105 s back to OFF. The tuning took ~15 s. Despite the signal fluctuation one can see how SRON decreases relative to SROFF by ca. 0.01 once the ON line seed laser wavelength is tuned to the center of the CO_2 absorption line.

For a given path length and optical power the GR precision is generally lower in the open atmosphere than quantified inside the closed laboratory. Figure 4(a) shows a GR, which for the same target distance, integration time and comparable optical power as for the indoor test in Fig. 2 fluctuates more than 10 times stronger. The acquisition took place around noon at clear sky and a temperature of 30 °C. A barren road was used as the hard target. The instrument, including receiver and transmitter, stood ca. 1 m above the ground. Through passively measuring the solar background signal we could exclude the latter from being the reason for the high GR fluctuation. This leaves turbulence related noise as the most likely cause. During daytime, under convective conditions, in the surface layer close to the ground there are typically extremes of turbulences [23]. Turbulently moving air was in fact visible with the bare eye. This example represents therefore an extreme case. We may obtain a figure of the expected noise through computation of the Rytov variance [24]. Using a path length of 22 m, a wavelength of 1573 nm and a refractive index structure constant for fairly strong turbulence $C_n^2 = 1 \times 10^{-13}$ $m^{-2/3}$ [21] yields a Rytov variance of 1.8×10^{-4}. This corresponds to a normalized STD of the received science signal intensity of $\sigma_I = 0.027$ [17], which approximately translates to the expected noise of the GR and indeed compares to the STD of the GR in Fig. 4(a).

Scintillation associated with atmospheric turbulence alters the signal on a scale of milliseconds [20,21]. Due to its statistical nature turbulence related noise may be reduced by averaging the data, provided the acquired data are statistically independent [20]. Accordingly, averaging the normalized samples of an ON/OFF pair and computing the GR improves the precision (standard error) slightly [Fig. 4(b)]. A further improvement, from 0.024 to 0.014, is achieved by increasing the number of ON/OFF pairs acquired per measurement and

#227072 - $15.00 USD Received 19 Nov 2014; revised 3 Jan 2015; accepted 3 Jan 2015; published 3 Mar 2015

computation of the GR values associated with each ON/OFF pair, followed by computing an average GR (ratio before average (RBA) method) [Fig. 4(b)]. Figure 4(c) illustrates how for a path length of 95 m the precision improves from 0.0126 (1 pair) to 0.0057 (1000 pairs). Figure 4(d) shows how for an 827 m long path the precision raises from 0.0136 (1 pair) to 0.0066 (2000 pairs).

Despite the different associated distances the precisions for Figs. 4(c) and 4(d) are comparable. Apart from the fact that the maximum integration times and the transmitted powers were different (400 mW and 1.5 W, respectively), this can be attributed to diverse atmospheric conditions and thus different power spectral densities of the refractive index fluctuations. For instance, the average propagation height for Fig. 4(d) was ~5 times higher (80 m) than for Fig. 4(c), thus the degree of turbulence was lower [17] and not significantly influenced by near surface turbulences. Furthermore, depending on the statistical independence of the data, averaging may have been more efficient in Fig. 4(d). Note that for all three cases the increase in precision does not follow a square root law, but is lower, which may indicate statistical dependence to some degree.

In spite of averaging the precision of a measurement in the open atmosphere is generally lower than in the closed laboratory, where atmospheric effects have been largely excluded. The associated uncertainties of the average background CO_2 mixing ratios are 1890 ppm, 178 ppm, and 28 ppm for Figs. 4(b), 4(c) and 4(d), respectively. In contrast, the instrument's precision of 0.00176 measured in the closed laboratory (Fig. 2) suggested corresponding uncertainties of only 237 ppm, 55 ppm and 6 ppm, respectively.

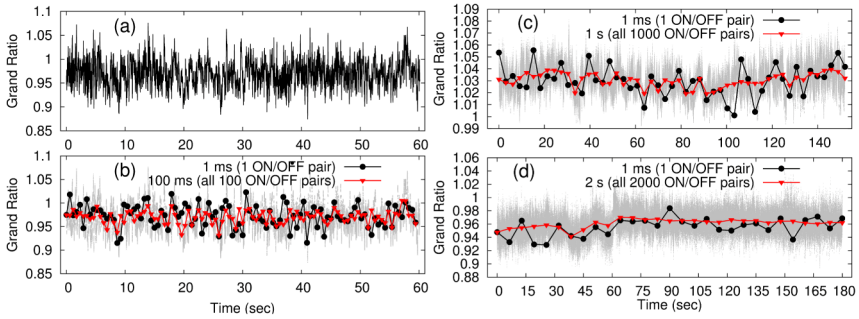

Fig. 4. Outdoor calibration tests. The wavelength switching rate was 2 kHz for all. (a) All GR values. The target was barren ground at 22 m distance. (b) Effect of averaging of (a). Standard error is 0.024 for an integration time of 1 ms (1 pair) and 0.014 for 100 ms (all 100 pairs) per point. (c) Weathered concrete hard target at 95 m distance. Standard error is 0.0126 for 1 ms and 0.0057 for 1 s integration time per point. (d) The target was a hill covered with bushes at 827 m distance. Standard error is 0.0136 for 1 ms and 0.0066 for 2 s integration time per point. GR values before averaging are displayed in grey.

4. Instrument test on Vulcano

Measurements on an actual volcano took place on July 16, 2014 on the island of Vulcano, Italy. The final objective is to not only measure CO_2 concentrations, but to obtain CO_2 fluxes. For this purpose the instrument eventually has to scan the plume. However, these pioneering tests were focusing on the more fundamental question whether the instrument would be able to acquire meaningful data at all in this dynamic and thus challenging environment.

Vulcano is a small volcanic island about 20 km north off the coast of Sicily and part of the Aeolian island arc [Fig. 5(a)]. The height of the volcano is 386 m a.s.l.. The instrument was placed at the flank of the crater, ca. 50 m north of the La Fossa crater rim [Fig. 5(b)] and was probing one of the fumaroles that were located at the crater slope. The fumaroles emit various volcanic gases, including CO_2 and water vapor. The latter condenses soon after it enters the atmosphere.

#227072 - $15.00 USD Received 19 Nov 2014; revised 3 Jan 2015; accepted 3 Jan 2015; published 3 Mar 2015

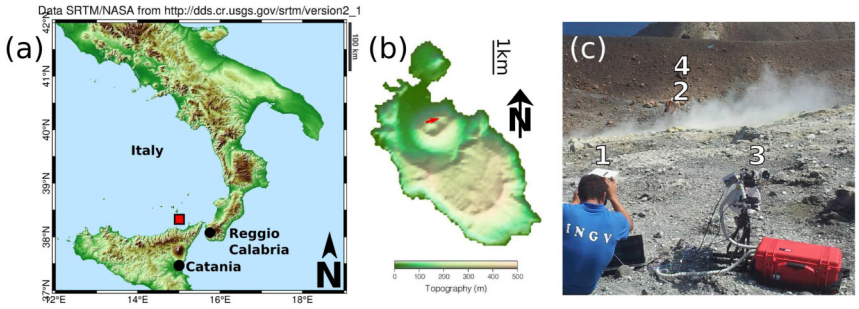

Fig. 5. (a) Location of Vulcano (red square). (b) Blowup of the island with the volcano in the northern part. The red arrow marks the measurement path, pointing towards east-northeast. (c) OP-FTIR (1), infrared source (2), compact DIAL (3) and hard target at 158 m distance (4). Condensed gas is visible.

For the given ON wavelength a parasitic volcanic absorbent may be H_2S gas, since its molecular absorption cross section is comparable to that of CO_2 at that spectral region [13]. However, for the fumaroles in that area the H_2S mixing ratio is so small compared with the background CO_2 mixing ratio [25] that no significant parasitic absorption due to H_2S is expected.

Measurements were carried out around 1 pm during a temperature of 30°C at clear sky. A steady wind of around 6 m/s was blowing up the crater flank such that the fumarole plume pointed towards the crater mouth and the laser beam crossed the plume at an angle of ca. 80 degrees. The fumarole diameter was estimated by the mean diameter of the condensed gas cloud and measured ~1.5 m from the ground up. The compact DIAL was operating at a wavelength switching rate of 1.25 kHz, acquiring 2000 ON/OFF pairs, corresponding to an integration time per measurement of 3.2 s, which amounts to 160000 science and 160000 reference samples. Figure 6(a) displays the complete ensemble of the inverse GR values before averaging, revealing a high variability. For reference, an open path Fourier spectrometer (OP-FTIR) [26] placed next to the compact DIAL [Fig. 5(c)] was measuring column averaged CO_2 concentrations. The measurement path length of the OP-FTIR was 26 m and included the fumarole at the end of the path. The latter was aligned with the path of the compact DIAL, which was pointing to a slope located 158 m away from the instrument. To enable an unambiguous range measurement the elevation angle of the compact DIAL was such that its laser beam crossed the fumarole about 0.5 m above the OP-FTIR line of sight. This ensured that most of the time light entering the telescope emanated from the target at 158 m and not from the condensed fumarole water vapor.

CO_2 concentrations are computed using Eq. (1) and the RBA method. The offset of the GR is corrected for by adjusting the minimum CO_2 concentrations with the corresponding concentrations from the OP-FTIR data. The differential absorption cross section of CO_2 is derived from Hitran 2012 spectroscopic data [13] using an air temperature of 303 K and a pressure of 970 mbar, measured at the meteorological station in Reggio Calabria. CO_2 concentrations are converted to mixing ratios using the dry air density. Figures 6(b) and 6(c) show the resulting time series of the path averaged CO_2 mixing ratios for the compact DIAL and the OP-FTIR, respectively. There is a correlation between the lower frequency components of the two time series. Note that the compact DIAL data was acquired with a higher temporal resolution (one point each 4 s) than the OP-FTIR data (one point each 11 s). While the CO_2 concentration obtained from the compact DIAL varies by up to 340% between minimum and maximum, the series from the OP-FTIR varies by up to 23% only. This can partly be explained by the fact that the two instruments were sensing a non-uniform CO_2 concentration and were not completely co-aligned, thus penetrating the plume at different points and under different angles.

#227072 - $15.00 USD Received 19 Nov 2014; revised 3 Jan 2015; accepted 3 Jan 2015; published 3 Mar 2015

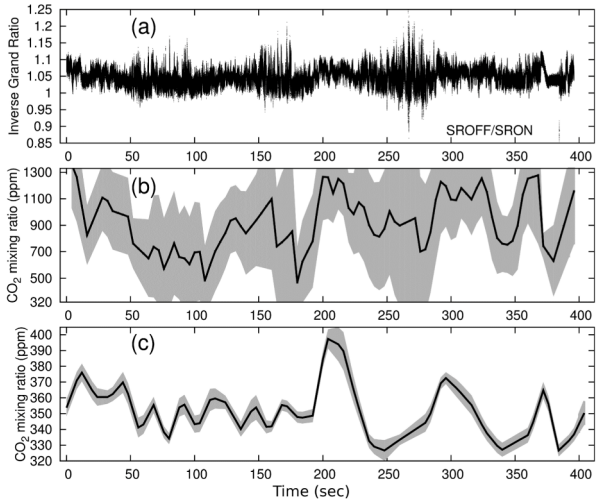

Fig. 6. Time series data from Vulcano. (a) Complete ensemble of inverse GR from the compact DIAL (inverse for enhanced comparability with Fig. 6(b)). (b) Path averaged CO_2 mixing ratios from compact DIAL. Grey envelope corresponds to ± STD of data in Fig. 6(a). (c) Path averaged CO_2 mixing ratios from OP-FTIR. Shaded grey depicts statistical error. To make them comparable in time, series in Figs. 6(b) and 6(c) have been gridded to a 4 s time interval.

If stroked by the laser the liquid water aerosol acts as a hard target with a rapidly changing reflectivity. Using Mie theory, assuming a droplet number density typical for a tropospheric liquid water cloud [27] and an immobile cloud during an ON/OFF period we computed the possible bias on the GR to be only 0.003%, corresponding to an error of the mixing ratio of 0.6 ppm.

More likely, turbulence-induced enhanced backscattering was the major cause of the poor quantitative agreement between the two time series. In particular,

(i) turbulence increased the non-uniformity of the already non-uniform CO_2 concentration near the fumarole and

(ii) noise was added by turbulence related effects.

Point (i) is in line with the finding of [11]. The OP-FTIR measurement path included the fumarole, but measured only 17% the length of the compact DIAL path. That means the reference measurement was in situ in the sense that it missed to probe 83% of the compact DIAL measurement path.

As stated in (ii), owing to turbulence the precision was significantly smaller than estimated under more calm atmospheric conditions. The disagreement between the mixing ratios of Figs. 6(b) and 6(c) is on average more than 400 ppm, which means two orders of magnitude higher than for the precision of 6 ppm, measured under calm indoor conditions, where atmospheric turbulence was almost completely excluded (Fig. 2). The disagreement is still an order of magnitude higher than the error measured for the test in Fig. 6d). Unlike for this case, however, the measurement conditions on Vulcano favored turbulence-induced enhanced backscattering. Near the fumarole the distance between the beam and the ground was less than 2 m. Furthermore, the beam propagated under an almost right angle to the wind, leading to a high degree of turbulence. In fact, the disagreement is comparable to the error in average CO_2 mixing ratio of the cases in Figs. 6(b) and 6(c), when translated to the 158 m path length on Vulcano.

The DIAL path length was relatively short. For the compact DIAL and a given target, spatial averaging of speckles is less efficient for shorter ranges as the illuminated target area and thus the speckle number is smaller. This may cause a considerable speckle noise bias. A rough analysis, neglecting any target properties, suggests a corresponding constant bias of ca. 0.01 in Fig. 6(a) [28], associated with a mixing ratio close to 200 ppm. Under the given

#227072 - $15.00 USD Received 19 Nov 2014; revised 3 Jan 2015; accepted 3 Jan 2015; published 3 Mar 2015

turbulent conditions, a speckle bias of this order of magnitude may have been transformed into a random fluctuation of the GR. However, this magnitude is before temporal averaging the data and thus rather an upper limit estimation.

Point (ii) could have contributed to the disagreement with the in situ measurement seen by [11] under windy conditions.

The employed separate wavelength emission technique assumes the atmosphere to be "frozen" [29] during the acquisition of an ON/OFF pair. Since there was a finite time of 0.8 ms between subsequent ON and OFF switching states this assumption is only approximately valid. Under the given atmospheric conditions, particularly upon occasional reflection off the liquid water aerosol, this may have amplified the discrepancy further.

5. Conclusion

We have presented a prototype of a compact DIAL for sensing volcanic CO_2 under harsh conditions, characterized it and demonstrated its operation in the field. We found that for this instrument neglecting atmospheric turbulence effects during error characterization may lead to an overestimated effective precision, the magnitude of which strongly depends on the measurement geometry and atmospheric conditions. For a test on a volcano on the island of Vulcano (Italy) the latter was likely causing poor precision of the grand ratio after averaging and thus a situation in which the CO_2 mixing ratio trend from the compact DIAL compared qualitatively well, but quantitatively poorly to corresponding in situ data. The result suggests two general interconnected implications, adding new experimental evidence to similar findings [11,16]. Firstly, an error analysis that neglects atmospheric effects may significantly overestimate the precision of DIAL instruments when used in a turbulent atmosphere. Secondly, under the latter conditions the DIAL result may largely disagree with an in situ reference measurement. This suggests that an in situ measurement is not an adequate reference for a DIAL in a turbulent atmosphere. As volcanic CO_2 signals are inherently non-uniform and often associated with an unstable atmosphere this has important implications for further developments of DIAL sensing volcanic CO_2. For instance, since the precision of the compact DIAL is most likely dominated by turbulence related noise, using a wavelength switching approach rather than dual wavelength emission, despite its simplicity, does not deem to be an optimum choice. As a consequence, the compact DIAL will be modified to allow for simultaneous transmission and measurement of ON and OFF wavelengths. This will also reduce noise due to a fast moving hard target or condensed water aerosol, which is important for future airborne measurements of volcanic plumes.

Acknowledgments

This work is financed by the European Research Council Grant 279802. More information under http://co2volc.pi.ingv.it. Our gratitude goes to Alessandro La Spina, Giuseppe Salerno and Francesco d'Amato (LENS) for assistance and helpful discussions.

#227072 - $15.00 USD Received 19 Nov 2014; revised 3 Jan 2015; accepted 3 Jan 2015; published 3 Mar 2015